Hyperpolarized ^{3}He Magnetic Resonance Imaging of Ventilation Defects in Healthy Elderly Volunteers: Initial Findings at 3.0 Tesla[1]

Grace Parraga, PhD, Lindsay Mathew, BMSc, Roya Etemad-Rezai, MD, David G. McCormack, MD, Giles E. Santyr, PhD

Rationale and Objectives. Hyperpolarized ^{3}He magnetic resonance imaging ventilation defects have been observed in subjects with respiratory disorders. We quantified ^{3}He ventilation defects in elderly and middle-aged subjects who had no history of smoking, respiratory, or cardiovascular disorders.

Materials and Methods. Hyperpolarized ^{3}He magnetic resonance imaging ventilation defect volume (VDV) and ventilation defect score (VDS) were assessed in eight elderly healthy volunteers (mean 67 ± 6 years) scanned twice within 7 ± 2 minutes and again 7 ± 2 days later. A younger cohort of 24 subjects (mean 44 ± 10 years) was also scanned for direct comparison. Four observers blinded to scan timepoint and subject identity scored VDS and manually segmented VDV in all center coronal slices.

Results. Center coronal slice ventilation defects were observed in six of eight elderly subjects (ages 63–74 years, 5 males) in all scans acquired and in no middle-aged subjects. At the scan timepoint, mean VDS was 2.7 (mean VDV 52 ± 34 cm^3), whereas for same-day rescan, mean VDS was 2.5 (mean VDV 53 ± 35 cm^3) and at 7-day rescan, mean VDS was 3.6 (mean VDV 48 ± 39 cm^3). Interscan coefficients of variation (COV) for mean VDV was 1.8% (same-day rescan) and 5.3% (7-day rescan) and interobserver COV ranged from 10–12%.

Conclusion. Elderly subjects have ventilation defects that are reproducible in same-day scanning and 7-day scanning visits. The observation of reproducible pulmonary ventilation defects in otherwise healthy elderly volunteers suggests caution must be used in interpreting results from ^{3}He studies of elderly subjects.

Key Words. Magnetic resonance imaging; ventilation defect; hyperpolarized ^{3}He.

New methods of pulmonary magnetic resonance imaging (MRI) with inhaled hyperpolarized helium-3 (^{3}He) have been shown to provide regional pulmonary ^{3}He ventilation maps and the location and size of ventilation changes within the lung in asthma (1–4), cystic fibrosis (5–10) and chronic obstructive pulmonary disease (COPD) (11–19). In patients with respiratory disease, areas of de-

Acad Radiol 2008; 15:776–785

[1] From Imaging Research Laboratories, Robarts Research Institute, 100 Perth Drive, London, ON, Canada, N6A 5K8 (L.M., G.E.S.); Department of Radiology and Nuclear Medicines (R.E.-R.), Department of Medical Biophysics (L.M., G.E.S.), and Department of Medicine, Division of Respirology, University of Western Ontario, London, ON, Canada (D.G.M.), The Lawson Health Research Institute, London, ON, Canada (D.G.M., G.P.); Department of Radiology, University Hospital, London Health Sciences Centre, London, ON, Canada (R.E.-R.). Received September 10, 2007; revised February 25, 2008; accepted March 18, 2008. L.M. was supported by the Schulich Graduate Research Fund provided by The University of Western Ontario (London, ON, Canada) and a Fellowship Award, from the Canadian Institutes of Health Research Cancer Research Training Program (London, ON, Canada). The study was supported by Imaging Research Laboratories, Robarts Research Institute (London, ON, Canada); The Departments of Radiology and Nuclear Medicine, Medical Biophysics, Department of Medicine (Division of Respirology), The University of Western Ontario (London, ON, Canada); Lawson Health Research Institute (London, ON, Canada); and the Department of Radiology, University Hospital (London, ON, Canada); the Ontario Research and Development Challenge Fund, the Canadian Institutes of Health Research, the Academic Medical Organization of Southwestern Ontario, as well as funding provided by the General Electric-London Health Sciences Centre Alliance Grant, Merck Frosst Canada Limited (Kirkland, PQ, Canada), and the Imaging Department at Merck Research Laboratories (Rahway, NJ). **Address correspondence to:** G.P. e-mail: gep@imaging.robarts.ca

doi:10.1016/j.acra.2008.03.003

creased ventilation from airflow changes are observed as "ventilation defects" that are visualized as decreased (and/or absence of) ^{3}He intensity in ^{3}He MRI spin density images.

Previously, both the size and number of these ventilation defects have been shown to correlate with severity in asthma (1–4), and in addition, exercise and methacholine challenge has been shown to alter the size, location, and number of defects that occur in asthma (3). We have also previously described a preliminary analysis of ventilation defect score (VDS) and ventilation defect volume (VDV) in 3 subjects: one with mild-moderate COPD, one with severe COPD, and a single healthy age-matched control (17). We noted in this study that significant ventilation defects were observed even in the healthy elderly subject. The finding of numerous center slice ventilation defects in an older healthy individual who was not a smoker, did not have asthma, or cardiovascular disease, and who had normal pulmonary function tests (17) was surprising and had not been reported previously in other studies of younger healthy volunteers. This result challenged us to explain the physiologic mechanisms related to ventilation defects in healthy lungs as well as the prevalence of ventilation defects in older and middle-aged individuals. To try to address some of these issues, the goal of this study was to examine and compare, using ^{3}He MRI, ventilation defects in elderly and middle-aged subjects who had no history of smoking, respiratory, or cardiovascular disease.

MATERIALS AND METHODS

Study Population

Subjects were recruited from the general population by newspaper advertisement and media coverage; they provided written informed consent to study protocols approved by The University of Western Ontario Standing Board of Human Research Ethics and by Health Canada. To qualify as a healthy subject, volunteers had to have no history of chronic respiratory disease or cardiovascular disease and less than 1 pack-year of smoking over their lifetime. In addition, subjects were enrolled based on forced expiratory volume in 1 second (FEV_1) $\geq$80% predicted and FEV_1 divided by the forced vital capacity (FVC) (FEV_1/FVC) $\geq$70%, measured using spirometry, according to the Global Initiative for Chronic Obstructive Lung Disease (GOLD) classification for healthy subjects (20). For the elderly cohort, subjects were recruited between the ages of 50 and 75 years and enrolled between the ages of 58 and 74 years inclusive, whereas for the younger subgroup, subjects were recruited between the ages of 18 and 60 years of age and enrolled between the ages of 23 and 57 years inclusive.

Spirometry

Spirometry was performed at screening and at each MRI visit using an *ndd EasyOne* spirometer (ndd Medizintchnik AG, Zurich, Switzerland) reporting forced FEV_1 (absolute and percent predicted) and FVC.

Magnetic Resonance Imaging

For both subject subgroups, MRI was performed on a whole body 3.0 Tesla Excite 12.0 MRS system (GEHC, Milwaukee, WI) with broadband imaging capability as previously described (17). All helium imaging employed a whole body gradient set with maximum gradient amplitude of 1.94 G/cm and a single channel, elliptic transmit/receive chest coil (RAPID Biomedical GmbH, Wuerzburg Germany). The basis frequency of the coil was 97.3 MHz and excitation power was 3.2 kW using an AMT 3T90 RF power amplifier (GEHC, Milwaukee, WI).

The elderly subgroup was scanned twice within 7 $\pm$ 2 minutes (scan and same-day rescan) and then again once within 7 $\pm$ 2 days (7-day rescan). All but two of the younger subjects were scanned on a single occasion only, with two subjects being scanned up to 20 times each within 2 years. Multislice ^{3}He coronal images were obtained using a fast gradient-echo method (FGRE) with centric k-space sampling (field-of-view [FOV] 40 $\times$ 40cm). Two interleaved images (echo time [TE] = 3.7 ms, relaxation time [TR] = 7.6 ms, 128 $\times$ 128, flip angle = 7°, 7 slices 30 mm thick), with and without additional diffusion sensitization (G = 1.94 G/cm, rise and fall time = 0.5 ms, gradient duration = 0.46 ms, Δ=1.46 ms, b value = 1.6 s/cm^2), were acquired for each slice with the non–diffusion-weighted image serving as a ^{3}He ventilation image for analysis. The total image acquisition time was 14 second. Each subject inhaled ^{3}He gas as previously described (17) from a 1 L ^{3}He/N_2 gas mixture consisting of a dose of 5 ml/kg of hyperpolarized ^{3}He [ie, for a 50-kg subject, 250 ml would be dispensed and diluted with medical N_2 to a total volume of 1 L, as previously described (19)]. The ^{3}He gas dose was administered to subjects after completing a tidal breath exhalation, and imaging was performed with the subject in breathhold, once the subject had completed inhaling the 1-L volume of gas. Proton imaging was performed after completion of ^{3}He imaging and subjects were scanned using a 4-channel radiofrequency coil

(GEHC, Milwaukee, WI) with the subject holding their breath after completing a tidal breath inhalation. Multislice ^{1}H coronal images were obtained using a fast spoiled gradient recalled echo sequence (256 × 256 matrix, FOV 40 ×40 cm, TR = 2.7, TE = 1.3, flip angle = 8°). All ^{1}H and ^{3}He scanning was completed within approximately 10 minutes of first lying in the scanner.

Hyperpolarized ^{3}He gas was provided by a turn-key, spin-exchange optical pumping system (HeliSpin™, GEHC, Durham, NC) as previously described (17).

Image Analysis

Center slice ^{3}He images were analyzed for VDS and VDV in a dedicated radiologic viewing room that provided a constant image visualization environment with consistent (darkened) room lighting. VDS and volumetric segmentation were performed for the center coronal slice only, determined by the presence of the carina, with the aid of the ^{1}H center-slice images (also identified by the presence of the carina). ^{3}He center-slice images were visually compared alone and registered together with ^{1}H center slice images. While all slices were reviewed, only the center coronal slice was quantitatively assessed, because in this study ^{1}H image slices were not acquired with the same slice thickness or breathhold as the ^{3}He images (slice thickness of 10 mm for ^{1}H compared to 30-mm slice thickness for ^{3}He). Rigid registration of the center coronal slice was based on the anatomic location of the carina.

Images were examined in the same image visualization environment by four trained observers for analysis of ventilation defects with all observers blinded to subject identity, disease status, and scan time-point. ^{3}He ventilation defects were identified according to a definition provided based on a previous study in asthma (2). Images were evaluated with a signal-to-noise (SNR) threshold of 22 and fixed contrast level, both of which were empirically established after reviewing all images. Images were reviewed such that for each subject all timepoints were displayed on a digital workstation monitor system (consisting of identical 19-inch flat panel monitors). Thus, all ^{3}He images for each subject were scored together with the observers blinded to the demographic, clinical, and spirometric information of the subjects. A ventilation defect was defined as previously described by Altes and coworkers (2) as any well-defined area of the lung showing no or low signal intensity compared with the remaining ventilated lung. Areas of absent signal associated with the pulmonary vascular structures, heart, hilum, and mediastinum were not considered to be ventilation defects. No lower boundary for defect size detection or quantification was used. After scoring ventilation defects, manual segmentation of the defects was performed on 32-bit image slices randomized together (subject and scan time) that were imported into a three-dimensional image visualization platform developed in our laboratory (21,22) for MR and ultrasound applications as previously described (23). The image visualization software tool used also provided a method for two-dimensional rigid image overlay or registration (of the center slice ^{1}H image and the center slice ^{3}He image, based upon the anatomic location of the carina), facilitating the manual segmentation of center-slice ventilation defect volume even in the case where poor registration occurred due to breathhold mismatch. As shown in Figure 1, two-dimensional image overlay (of the center slice ^{1}H image and the center slice ^{3}He image) facilitated the identification and manual segmentation of center slice ventilation defects. ^{3}He ventilation defects were manually segmented, recorded, and multiplied by the slice thickness (30 mm) to provide an estimate of center slice VDV, which was recorded in dedicated source documents. Interscan and interobserver variability were assessed using the coefficient of variation (COV), which was calculated as the standard deviation of the difference (between scans for interscan and between observers for interobserver) divided by mean VDV.

RESULTS

Study Subjects

Eight elderly healthy subjects (five males) were enrolled (mean age 67 ± 6 years, range 58–74) as well as 24 (14 males) middle-aged healthy volunteers (mean age 44 ± 10 years, range 23–57). Baseline subject demographic data and pulmonary function test results are reported in Table 1. Both subgroups had similar baseline mean weight, FEV_1 (% predicted) and FEV_1/FVC. None of the subjects had a history of cardiovascular or respiratory disorders, obesity, sleep disorders, and none of the subjects had smoked within the last 10 years or had a smoking history of >1 pack-year over their lifetime. Body mass indexes ranged from 24–35 kg/m^2 for the elderly subjects and 20–24 kg/m^2 for the middle-aged subjects. The two subgroups had significantly different mean age (P <.001). All subjects, except for a single elderly subject who withdrew from the 7-day scanning visit due to claustrophobia, were able to complete all scans and

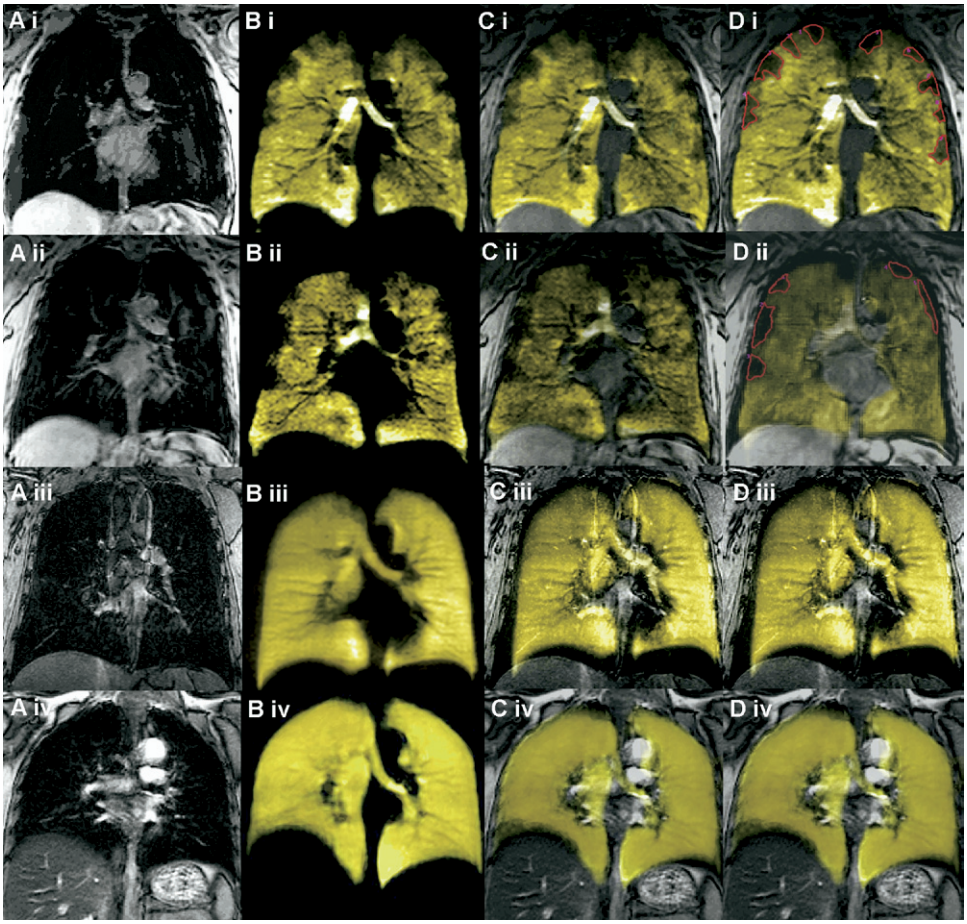

Figure 1. Hyperpolarized ^{3}He magnetic resonance imaging ventilation defect volume segmentation approach. **(a)** ^{1}H thoracic cavity: (i) Subject 7-1003, (ii) Subject 7-1008, (iii) Subject 6-007, (iv) Subject 6-001. **(b)** Hyperpolarized ^{3}He ventilation image: (i) Subject 7-1003, (ii) Subject 7-1008, (iii) Subject 6-007, (iv) Subject 6-001. **(c)** Overlay of ^{3}He ventilation image (yellow) on ^{1}H thoracic cavity (grey): (i) Subject 7-1003, (ii) Subject 7-1008, (iii) Subject 6-007, (iv) Subject 6-001. **(d)** Segmentation of ^{3}He ventilation defects (red): (i) Subject 7-1003, (ii) Subject 7-1008, (iii) Subject 6-007, (iv) Subject 6-001.

visits. The single subject who withdrew after his first scanning visit was scanned twice during his single scanning visit. Two middle-aged healthy subjects were scanned up to 20 times each within two years.

Ventilation Defects and Ventilation Defect Volume

As shown in Tables 1 and 2, none of the middle-aged healthy volunteers showed evidence of center coronal slice ^{3}He ventilation defects, including two of these subjects who were scanned up to 20 times each within a two-year time frame. Although only the center slice was quantitatively assessed, for these younger subjects, ventilation defects were not observed in any slices. However, six of eight elderly healthy volunteers exhibited visibly obvious ^{3}He ventilation defects in scans acquired at baseline scan, same-day rescan, and 7-day rescan (Table 2). Two of the eight healthy elderly subjects had no ventilation defects in any slice during scan, same-day rescan, or 7-day rescan; these were both male subjects and the youngest in the subgroup (age 58, BMI 27 kg/m^2 and age 60, BMI 35 kg/m^2, respectively). For all healthy elderly subjects, mean center slice VDS was 2.5. For all healthy elderly subjects, mean center slice was 2.7 at scan and 2.5 for same day re-scan, whereas for 7-day rescan, VDS was 3.6. Mean center slice VDV was 52 $\pm$ 34 cm^3 at scan, 53 $\pm$ 35 cm^3 at same-day rescan, and 48 $\pm$ 39 cm^3 at 7-day rescan. Figure 2 shows ^{3}He ventilation images with defects identified with arrows (Fig. 2(i)) and the overlay of ^{3}He ventilation images on the ^{1}H thoracic cavity image (Fig. 2(ii)) for three representative healthy elderly subjects (ages 70, 73,

Table 1
Study Subject Demographic Characteristics

	Elderly Healthy Volunteers (n = 8)	Middle-aged Healthy Volunteers (n = 24)
Male (n)	5	14
Age (± SD) [range] (yrs)	67 (6) [58–74]	44 (10) [23–57]
Weight (± SD) kg	76 (17)	76 (13)
Body mass index (± SD) [range]	27 (4) [24–35]	25 (3) [20–34]
FEV_1 % predicted (± SD)	106 (19)	101 (11)
FEV_1/FVC % (± SD)	77 (5)	80 (8)
Subjects with ventilation defects (n) (male)	6 (3)	0 (0)
Total ventilation defects (n)		
Scan	16	0
Same-day rescan	15	0
7-day Rescan	18	0
Mean VDV cm^3 (± SD)		
Scan	52 (34)	0
Same-day rescan	53 (35)	0
7-day rescan	48 (39)	0

SD, subgroup standard deviation for eight healthy volunteers; FEV, forced expiratory volume in 1 second; FVC, forced vital capacity.

Table 2
Ventilation Defects in Elderly Healthy Volunteers

	Ventilation Defects in Center Slice		
	Scan	Same-day Rescan	7-day Rescan
Subject 1001 (n)	0	0	0
Subject 1002 (n)	3	3	ND
Subject 1003 (n)	3	3	5
Subject 1004 (n)	2	2	4
Subject 1005 (n)	3	2	3
Subject 1006 (n)	0	0	0
Subject 1007 (n)	2	2	3
Subject 1008 (n)	3	3	3
Total sum defects	16	15	18
Mean defect score	2.7	2.5	3.6

ND, not done (patient withdrew from study due to claustrophobia)

and 74 years, respectively). Figure 3 provides representative ^{3}He ventilation scans for three representative healthy middle-aged subjects (ages 45, 43, and 39 years, respectively). The range of SNR for the images in both subgroups was similar.

Ventilation Defect Volume Interscan and Interobserver Reproducibility

For all eight elderly subjects who underwent scanning, interscan COV for mean VDV was 1.8% for same-day scanning and 5.3% for 7-day scanning. Figure 4 shows ^{3}He ventilation images providing visual evidence of the reproducibility of VDV for two representative elderly subjects with ventilation defects that completed both same-day and 7-day scanning visits. For both subjects, the magnitude and location of many of the defects are very similar during same-day scanning; there are a few differences in the number of defects, the location of the defects, and the size of the defects observed in the 7-day rescan. For comparison, repeated scans of two middle-aged subjects are also provided in Figure 4 with rescan performed within 8 months of baseline and the second rescan performed within 2 years of baseline. No defects or visual differences were observed in the scans for the middle-aged subjects. Although a single observer's results are provided in Table 1, the results for three additional observers are provided in Table 3 as well as interobserver COV, which ranged from 10–12%.

DISCUSSION

A number of important observations were made in this study. First, all subjects in this study who were 63 years of age and older displayed ventilation defects in the center coronal slice, and the number, location, and size of these defects were highly reproducible for same day scanning sessions with mean interscan VDV COV 1.8% and mean VDS of 2.7 and 2.5. Somewhat lower reproducibility was observed for the 7-day scanning visit compared to baseline, with a mean interscan VDV COV of 5.3% and mean VDS of 3.6 defects. However, all of the six elderly subjects who displayed ventilation defects at baseline displayed very similar number and size of ventilation defects at the 7-day scanning session. In addition, none of the 24 healthy volunteers in the middle-aged subgroup displayed ventilation defects during any scanning session and neither did the two youngest subjects in the elderly subgroup. As shown in Table 3, four observers measured VDV over a 1.5-year period with interobserver COV ranging from 10–12%. In recent work, Altes and coworkers (24) showed the association of age and ventilatory defects, which supports the finding reported here of

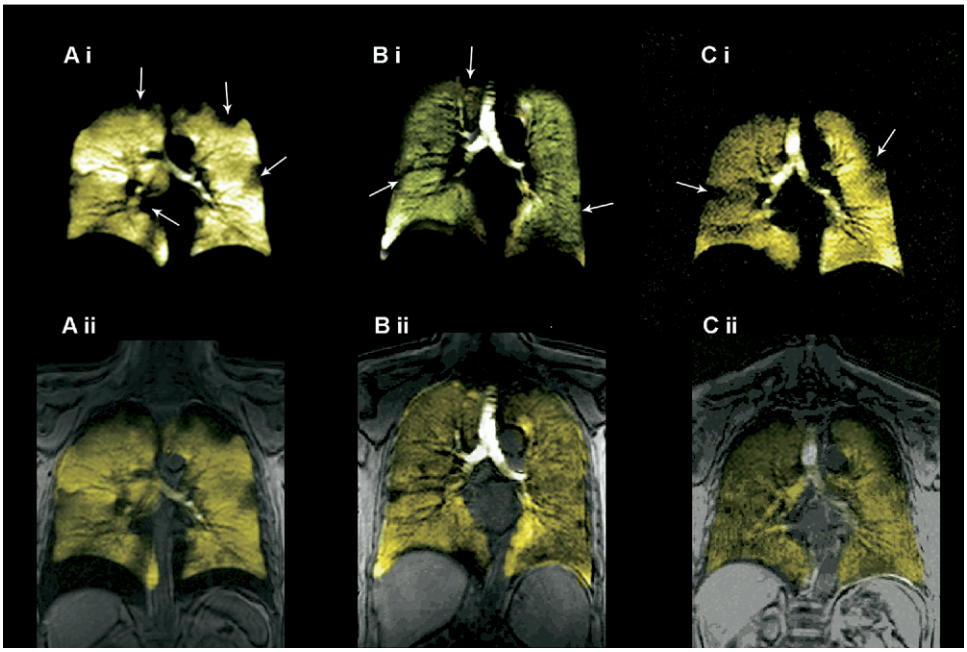

Figure 2. Elderly healthy volunteers ^{3}He magnetic resonance imaging. **(a)** Subject 7-1004 70-year-old female, forced expiratory volume in 1 second (FEV_1) = 149% predicted, FEV_1/ forced vital capacity (FVC) = 75% (i) ^{3}He image (ii) overlay of ^{3}He image with ^{1}H thorax image. **(b)** Subject 7-1007 73-year-old male, FEV_1 = 104% predicted, FEV_1/FVC = 84%. (i) ^{3}He image (ii) overlay of ^{3}He image with ^{1}H thorax image. **(c)** Subject 7-1008 74-year-old male, FEV_1 = 91% predicted, FEV_1/FVC=79% (i) ^{3}He image (ii) overlay of ^{3}He image with ^{1}H thorax image.

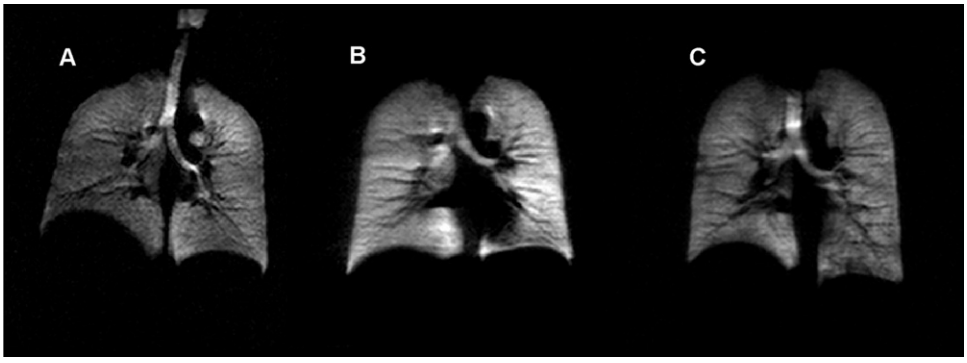

Figure 3. Middle-aged healthy volunteers ^{3}He magnetic resonance imaging. **(a)** Subject 6-1001 45-year-old female. **(b)** Subject 6-1003 42-year-old male. **(c)** Subject 6-1010 39-year-old male.

significantly different size and number of defects in the center coronal slice of healthy younger and elderly volunteers. Their previous work also reported small mean numbers (<2) of ventilation defects in younger healthy volunteers (6) when the entire lung was assessed. In current studies of healthy volunteers at 3.0 Tesla at our site, there is little evidence of posterior or other slice defects in healthy volunteers who have less than 1 pack-year smoking and no evidence of cardiovascular or respiratory disease. This may be the case because ^{3}He MRI at our site has been limited to less than 50 healthy volunteers; it is possible that with more subjects scanned, ventilation defects will be detected.

A second finding from this preliminary study was that for the six elderly subjects for whom defects were observed, there was a tendency for these to appear in the same locations 7 days later. In some cases, the original defects were accompanied by new defects and/or slightly altered sizes. Regional persistence or recurrence of ventilation defects has also been recently described in asthma

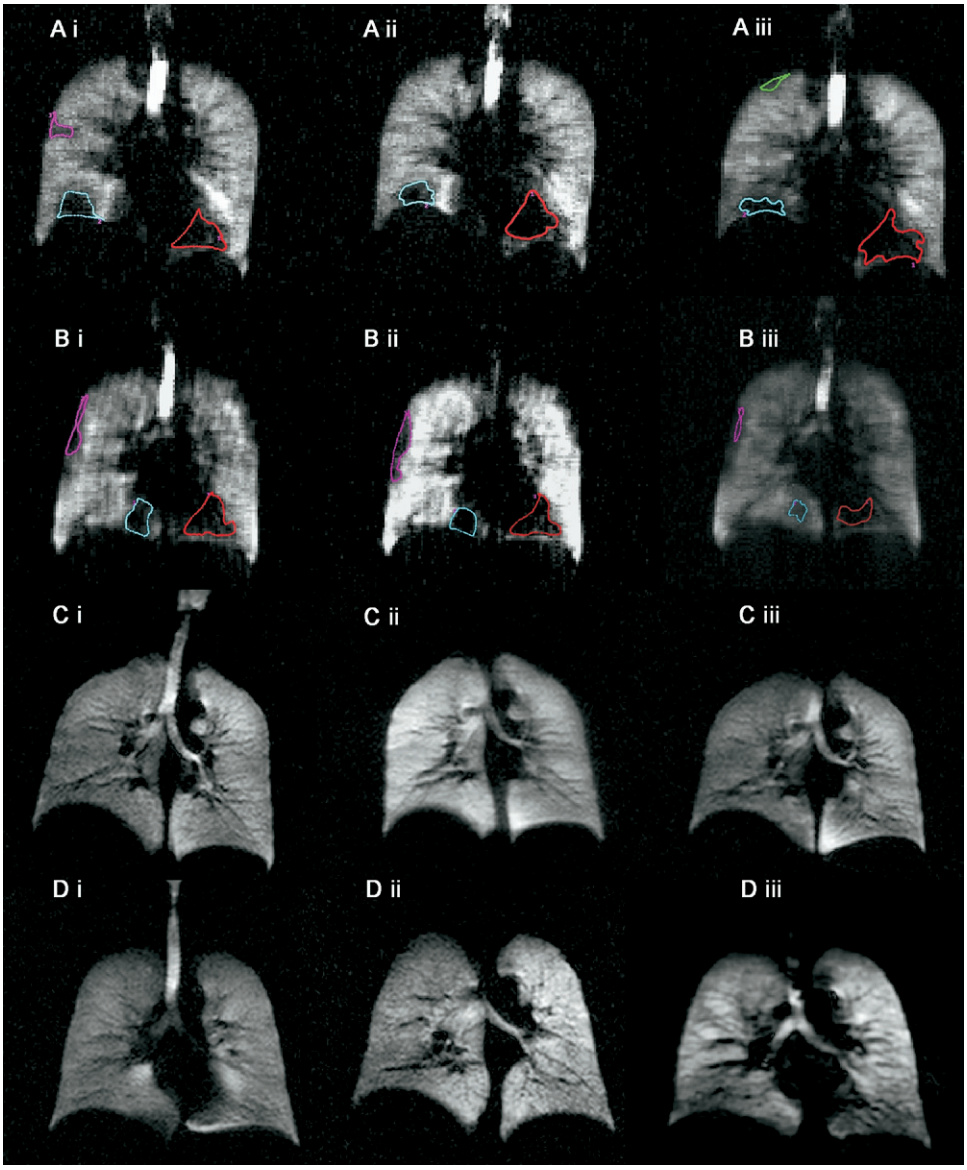

Figure 4. Reproducibility of ^{3}He ventilation in elderly and middle-aged healthy volunteers. **(a)** Subject 7-1005 elderly volunteer: (i) scan, (ii) same-day rescan, (iii) 7-day rescan. **(b)** Subject 7-1008 elderly volunteer: (i) scan, (ii) same-day rescan, (iii) 7-day rescan. **(c)** Subject 6-1001 middle-aged volunteer: (i) scan, (ii) rescan 1, (iii) rescan 2. **(d)** Subject 6-1002 middle-aged volunteer: (i) scan, (ii) rescan 1, (iii) re-scan 2.

by Altes et a; (2) with specific regions of the lung appearing to be more likely to display altered ventilation patterns. The observation in this study that regional persistence is also a feature of ventilatory defects in healthy elderly subjects suggests that specific airways appear to be preferentially closed in the aging lung and that these airways are more likely to be closed on sequential days. It is important to point out that all subject scanning sessions were scheduled for the same time of day on the second scanning visit as the first scanning visit ($\pm$1 hour from baseline scan for each subject) and always during mid-morning. Spirometry measurements were also recorded before and after each scanning session, and there was no change in spirometry measures observed for any subjects between scanning dates or after MR scanning. Finally, obesity is a critical issue to consider when imaging subjects in the supine position, as extra weight directly influences respiratory mechanics in the supine and

Table 3
Elderly Volunteer Ventilation Defect Volume Interobserver Reproduciblity

	Mean VDV cm^3 (± SD)		
	Scan	Same-day Rescan	7-day Rescan
Observer 1	52 (34)	53 (35)	48 (39)
Observer 2	72 (55)	67 (47)	60 (48)
Observer 3	67 (43)	64 (42)	53 (40)
Observer 4	70 (63)	65 (61)	46 (44)
Mean Ob1-4	66 (8)*	62 (6)*	52 (6)*
COV (%)	12	10	12

SD, subgroup standard deviation for eight healthy volunteers, except for *SD is observer standard deviation; COV, *SD/ mean VDV for observers.

upright position. None of the subjects who displayed ventilation defects were obese; hence, it is unlikely that any of the ventilatory defects observed were related to BMI.

Thirdly, we observed that for the elderly healthy volunteers, all defects in the center coronal slice appeared on the periphery of the coronal slice, which is similar to previously published work in asthma (1–4). This finding of peripheral lung ventilation defects in the elderly healthy lung and in asthma is in contrast to previously published ^{3}He results for subjects with COPD for us (17) and others (11–16,18,19) and in cystic fibrosis (7–10), where numerous and large defects are observed throughout the coronal and axial plane and not on the periphery alone.

The primary limitation of this preliminary study is the small sample size of the elderly subject group and the fact that for the majority of the middle-aged subjects group there was no protocol specification for prospective repeated scanning because no ventilation defects were observed at baseline. For two middle-aged subjects, repeated scanning was undertaken, only because these subjects were enrolled in a hardware and software development protocol requiring multiple scanning visits to enable pulse programming alteration assessments. Both of these subjects were scanned up to 20 times over two years and these subjects (both with ages very close to the mean of the middle-aged group) never displayed ventilation defects during any scanning visit. Another limitation of the study is related to the fact that subjects were scanned in a study designed to assess the reproducibility of the ^{3}He apparent diffusion coefficient (ADC) and hence the images had lower SNR and thicker slices than the spin density images. The elderly subjects were enrolled in the present study with ADC reproducibility as the primary endpoint, and as such, the protocol utilized an optimized ADC sequence. The primary focus on ADC required necessary trade-offs be made in the use of the non–diffusion-weighted images as an indication of ventilation (ie, increased TE, diffusion time). We acknowledge that the longer TE would introduce undesirable T2* weighting into the ventilation, but expect that this effect would lead to less than 50% signal reduction even with the largest ADC (larger airways). The signal in the airways is well appreciated in our images. Therefore, this suggests that the regions of signal void in the lung parenchyma attributed to ventilation defect in this study represent the absence of helium gas and not signal decay. This is confirmed by the measurement of the same signal voids in spin density images (obtained on visit 2 only, data not shown), which was obtained with TE of about half that of the non–diffusion-weighted images.

Another limitation of this study is the fact that ^{3}He and ^{1}H images were acquired at somewhat different lung volumes and that this likely influenced the accuracy of ventilation defect segmentation along the lung-pleura boundaries. For example, the ^{1}H images were acquired after tidal breathing with instructions to the subjects to hold their breath at the top of tidal volume. The ^{3}He images were acquired after tidal breathing and breathhold after inhaling 1 L of the ^{3}He/N_2 gas mixture. Therefore, the breathhold volumes were not exactly matched and rigid registration of ^{3}He and ^{1}H images was not perfect in some cases. However, although the images were acquired at slightly different volumes, the lung boundaries were readily discerned when the ^{1}H and ^{3}He images are provided in overlay and identification of these are facilitated in all six cases where there were clear ventilation defects at the outer boundary of the lungs. Because ^{1}H and ^{3}He images were not acquired with exactly matching breathholds and very different slice thickness, we limited the analysis of defect volume reproducibility to the center coronal slice where the edge of the thoracic cavity and ventilation defects were most easily discerned. Hence, in this study, center coronal slice VDV represented the area of ventilation defect for the center slice, which was then multiplied by the 30-mm slice thickness to reflect estimated contributions from the entire slice. Because of the rather thick slices used, center slice VDV as measured in this study, although an adequate indicator of measurement precision, provides only an estimate of the true ventilation defect volume. The use of thinner slices and three-dimensional imaging approaches will allow for an estimate of VDV that is likely more accurate. We also point out that

for some subject images, the apexes of the lung have complex ventilation patterns that might be interpreted as ventilation defects. In most cases, the overlay of proton and helium images allows for interpretation of the irregular shape of the ventilation image as dependent upon tissue and bone anatomy at the top of the lung. We investigated coil coverage and found that there is excellent signal intensity in the trachea up to and including the cricoid/larynx. We have also directly quantified coil inhomogeneity (25) as less than 20% in the superior-inferior direction over a 44-cm FOV, which is likely adequate for the imaging results we have presented here.

Why do elderly healthy volunteers display ^{3}He MRI ventilation defects along the periphery of the coronal plane of the lung? How is this finding related to the increased ADC values shown previously for older subjects at our center and others (4,17,26) and in the six elderly subjects in this study with ventilation defects (with mean ADC = 0.27 cm^2/s)? How might this finding be related to other measurements of pulmonary physiology that are also known to change with aging such as FEV_1 and closing volume? It is possible that along with changes in the lung airspaces such as alveoli and acinar ducts, (as evidenced by increased ADC) changes in airways may also occur over time. In this study, the majority of defects were observed along the periphery of the coronal slice, which suggests that terminal airway closure or narrowing may be an age-dependent pathology of the lung. Altes and co-workers (24) have also observed ventilation defects in healthy volunteers are positively correlated with age, suggesting that the finding here in a few elderly subjects should be assessed in more volunteers in multicenter studies. Although the etiology of ventilation defects is yet unknown, we are currently assessing the presence and reproducibility of ventilation defects in a greater number of elderly COPD subjects and elderly (age-matched) healthy volunteers over a five-year period to better understand this radiologic finding. The observation of reproducible pulmonary ventilation defects in otherwise healthy elderly volunteers suggests caution must be used in interpreting results from ^{3}He studies of elderly subjects with underlying disease. This finding further suggests that inclusion of a healthy elderly volunteer control group may be required when using ^{3}He MRI in treatment studies of elderly subjects with COPD to appropriately relate potential treatment effects to underlying disease and not other processes related to aging. If the results of this preliminary study are observed in the majority of elderly volunteers scanned in our laboratory and elsewhere, this may potentially result in increased subject sample sizes required in cohort and treatment studies of elderly subjects with respiratory disease where ^{3}He MRI phenotypes are used as measurements or biomarkers of disease.

CONCLUSIONS

In conclusion, the observations made in this study of a relatively small group of elderly and middle-aged healthy volunteers indicated that regional ventilation defects within the lung as demonstrated using ^{3}He MRI were present in six elderly subjects aged 63–74 years. These ventilation defects were highly reproducible in size and location in repeated scans within a few minutes and again 7 days later. These results suggest that as part of the aging processes in the lung, nonrandom airway closure or narrowing occurs that is restricted to the lung periphery and is regionally recurrent or persistent. The results further suggest that these airway changes are occurring in the absence of known or detectable respiratory or cardiovascular disease, perhaps as part of normal aging processes. Further work is required to unravel the etiology of these defects in healthy elderly volunteers.

ACKNOWLEDGEMENTS

The authors thank Sandra Halko, Shayna McKay, and Christine Piechowicz for clinical coordination and clinical database management; Jessica McCallum for assistance with image analysis; Wilfred Lam for production and dispensing of ^{3}He gas, as well as Elisabeth Lorusso, RMT, and Cyndi Harper-Little, RMT, for MR scanning of research volunteers. Special thanks to Dr. Aaron Fenster for helpful discussions. The use of an onsite hyperpolarized ^{3}He gas polarizer system (HeliSpin™, General Electric Health Care (GEHC), Durham, NC) was provided to Robarts Research Institute by Merck through an agreement between GEHC and Merck.

REFERENCES

1. Altes TA, Powers PL, Knight-Scott J, et al. Hyperpolarized ^{3}He MR lung ventilation imaging in asthmatics: preliminary findings. J Magn Reson Imaging 2001; 13:378–384.
2. de Lange EE, Altes TA, Patrie JT, et al. The variability of regional airflow obstruction within the lungs of patients with asthma: assessment with hyperpolarized helium-3 magnetic resonance imaging. J Allergy Clin Immunol 2007; 119:1072–1078.
3. Samee S, Altes T, Powers P, et al. Imaging the lungs in asthmatic patients by using hyperpolarized helium-3 magnetic resonance: assessment of response to methacholine and exercise challenge. J Allergy Clin Immunol 2003; 111:1205–1211.

4. de Lange EE, Altes TA, Patrie JT, et al. Evaluation of asthma with hyperpolarized helium-3 MRI: correlation with clinical severity and spirometry. Chest 2006; 130:1055–1062.
5. Altes TA, de Lange EE. Applications of hyperpolarized helium-3 gas magnetic resonance imaging in pediatric lung disease. Top Magn Reson Imaging 2003; 14:231–236.
6. Altes TA, Eichinger M, Puderbach M. Magnetic resonance imaging of the lung in cystic fibrosis. Proc Am Thorac Soc 2007; 4:321–327.
7. Donnelly LF, MacFall JR, McAdams HP, et al. Cystic fibrosis: combined hyperpolarized ^{3}He-enhanced and conventional proton MR imaging in the lung-—preliminary observations. Radiology 1999; 212:885–889.
8. Koumellis P, Van Beek EJ, Woodhouse N, et al. Quantitative analysis of regional airways obstruction using dynamic hyperpolarized ^{3}He MRI-preliminary results in children with cystic fibrosis. J Magn Reson Imaging 2005; 22:420–426.
9. Mentore K, Froh DK, de Lange EE, et al. Hyperpolarized HHe 3 MRI of the lung in cystic fibrosis: assessment at baseline and after bronchodilator and airway clearance treatment. Acad Radiol 2005; 12: 1423–1429.
10. Salerno M, Altes TA, Brookeman JR, et al. Dynamic spiral MRI of pulmonary gas flow using hyperpolarized (3)He: preliminary studies in healthy and diseased lungs. Magn Reson Med 2001; 46:667–677.
11. Ebert M, Grossmann T, Heil W, et al. Nuclear magnetic resonance imaging with hyperpolarised helium-3. Lancet 1996; 347:1297–1299.
12. Fain SB, Panth SR, Evans MD, et al. Early emphysematous changes in asymptomatic smokers: detection with ^{3}He MR imaging. Radiology 2006; 239:875–883.
13. Kauczor HU, Hofmann D, Kreitner KF, et al. Normal and abnormal pulmonary ventilation: visualization at hyperpolarized He-3 MR imaging. Radiology 1996; 201:564–568.
14. Ley S, Zaporozhan J, Morbach A, et al. Functional evaluation of emphysema using diffusion-weighted 3Helium-magnetic resonance imaging, high-resolution computed tomography, and lung function tests. Invest Radiol 2004; 39:427–434.
15. MacFall JR, Charles HC, Black RD, et al. Human lung air spaces: potential for MR imaging with hyperpolarized He-3. Radiology 1996; 200:553–558.
16. Morbach AE, Gast KK, Schmiedeskamp J, et al. Diffusion-weighted MRI of the lung with hyperpolarized helium-3: a study of reproducibility. J Magn Reson Imaging 2005; 21:765–774.
17. Parraga G, Ouriadov A, Evans A, et al. Hyperpolarized ^{3}He ventilation defects and apparent diffusion coefficients in chronic obstructive pulmonary disease: preliminary results at 3.0 Tesla. Invest Radiol 2007; 42:384–391.
18. Swift AJ, Wild JM, Fichele S, et al. Emphysematous changes and normal variation in smokers and COPD patients using diffusion ^{3}He MRI. Eur J Radiol 2005; 54:352–358.
19. Woodhouse N, Wild JM, Paley MN, et al. Combined helium-3/proton magnetic resonance imaging measurement of ventilated lung volumes in smokers compared to never-smokers. J Magn Reson Imaging 2005; 21:365–369.
20. Pauwels RA, Buist AS, Calverley PM, et al. Global strategy for the diagnosis, management, and prevention of chronic obstructive pulmonary disease. NHLBI/WHO Global Initiative for Chronic Obstructive Lung Disease (GOLD) Workshop summary. Am J Respir Crit Care Med 2001; 163:1256–1276.
21. Landry A, Spence JD, Fenster A. Measurement of carotid plaque volume by 3-dimensional ultrasound. Stroke 2004; 35:864–869.
22. Landry A, Fenster A. Theoretical and experimental quantification of carotid plaque volume measurements made by three-dimensional ultrasound using test phantoms. Med Phys 2002; 29:2319–2327.
23. Landry A, Spence JD, Fenster A. Quantification of carotid plaque volume measurements using 3D ultrasound imaging. Ultrasound Med Biol 2005; 31:751–762.
24. Choudhri A, Altes, TA, Stay R, et al. The Occurence of Ventilation Defects in the Lungs of Healthy Subjects as Demonstrated by Hyperpolarized Helium-3 MR Imaging. RSNA SSA21-05. 2007.
25. Ouriadov A, Etemad-Rezai R, Parraga G, Santyr GE. Correction of errors due to RF field inhomogeneities in hyperpolarized ^{3}He measurement of alveolar oxygen partial pressure in human lung. 2008. Toronto. Proceedings of the 16th Annual Scientific Meeting of the International Society for Magnetic Resonance in Medicine. Toronto; 2008.
26. Fain SB, Altes TA, Panth SR, et al. Detection of age-dependent changes in healthy adult lungs with diffusion-weighted ^{3}He MRI. Acad Radiol 2005; 12:1385–1393.